Multiscale finite element methods for miscible and immiscible flow in porous media

Ruben Juanes
Tadeusz W. Patzek

Department of Civil and Environmental Engineering
University of California at Berkeley
631 Davis Hall, Berkeley, CA 94720-1710

Abstract

In this paper we study the numerical solution of miscible and immiscible flow in porous media, acknowledging that these phenomena entail a multiplicity of scales. The governing equations are conservation laws, which take the form of a linear advection-diffusion equation and the Buckley-Leverett equation, respectively. We are interested in the case of small diffusion, so that the equations are almost hyperbolic. Here we present a stabilized finite element method, which arises from considering a multiscale decomposition of the variable of interest into resolved and unresolved scales. This approach incorporates the effect of the fine (subgrid) scale onto the coarse (grid) scale. The numerical simulations clearly show the potential of the method for solving multiphase compositional flow in porous media. In particular, the results for the Buckley-Leverett problem are unparalleled.

KEY WORDS: flow in porous media, conservation laws, multiscale phenomena, finite elements, stabilized methods

1 Introduction

One of the main difficulties when solving flow and transport in fractured porous media stems from the fact that, very often, these processes are *not* dominated by diffusion. This makes the mathematical problem almost hyperbolic, which naturally develops sharp features in the solution. Classical numerical methods produce a solution that either lacks *stability*, resulting in nonphysical oscillations, or *accuracy*, by showing excessive numerical diffusion.

A huge number of publications, which we do not attempt to review here, has emerged to provide a solution to this fundamental problem. Despite the attention advection-dominated flow has received from the scientific community in the past decades, there is still a need for new numerical techniques. Modern characteristics methods like Eulerian-Lagrangian Localized Adjoint Methods (ELLAM) [7] require a fine grid to accurately track the characteristics in a highly nonlinear problem, and state-of-the-art stabilized methods like Streamline-upwind/Petrov-Galerkin (SUPG) [5] or Galerkin Least Squares (GLS) [16], are not as effective in the presence of reaction and production terms [10].

Development of novel numerical methods for the complete equations of multiphase compositional flow in multidimensions must necessarily start from simplified models in one space dimension. These reduced model problems should display, however, the key features which pose difficulties in obtaining satisfactory numerical solutions such as, for instance, wild nonlinearity, shocks or near-shocks, boundary layers and degenerate diffusion. The key point of the proposed formulation is a multiscale decomposition of the variable of interest into resolved (or grid) scales and unresolved (or subgrid) scales, which acknowledges the fact that the fine-scale structure of the solution cannot be captured by *any* mesh. However, the influence of the subgrid scales on the resolvable scales is not negligible. By accounting for the subgrid scales, the oscillatory behavior of classical Galerkin is drastically reduced and confined to a small neighborhood containing the sharp features, while the solution is high-order accurate where the solution is smooth. This ensures that

the numerical solution is not globally deteriorated. The method does *not* emanate from a monotonicity argument and, therefore, it does not rule out small overshoots and undershoots near the sharp layers. These localized wiggles could be removed using a shock-capturing technique (see, *e.g.*, [9] and the references therein).

The mathematical and numerical formulations are described in Section 2, within the unified framework of conservation laws. Under certain simplifying assumptions, miscible flow takes the form of a linear advection-diffusion equation, while immiscible flow leads to the classical Buckley-Leverett equation. Several representative numerical simulations for both miscible and immiscible flow are presented in Section 3. In Section 4 we draw the main conclusions of this investigation.

2 Numerical formulation

2.1 Initial and boundary value problem

We shall understand miscible and immiscible flow in porous media as scalar conservation laws of the form [8]:

$$\partial_t u + \nabla \cdot \boldsymbol{\mathcal{F}} = q, \quad x \in \Omega,\ t \in (0, T], \tag{1}$$

where u is the conserved quantity, $\boldsymbol{\mathcal{F}}$ is the total flux of that quantity, q is the rate of production (per unit volume), Ω is the spatial domain and $(0, T]$ is the time interval of interest. With the usual notation, $\partial_t(\cdot)$ refers to partial derivative with respect to time. The total flux has the form [8, 12, 13]:

$$\boldsymbol{\mathcal{F}} = \boldsymbol{f}(u) - \mathbf{D}(u)\nabla u, \tag{2}$$

where $\boldsymbol{f}$ is the hyperbolic part of the flux and $\mathbf{D}$ is the diffusion tensor. Both are allowed to be nonlinear functions of the unknown u. For expositional simplicity, we consider homogeneous Dirichlet boundary conditions only:

$$u = 0 \text{ on } \partial\Omega, \tag{3}$$

where $\partial\Omega$ is the boundary of the domain. The initial conditions are

$$u(x, t = 0) = u_0(x). \tag{4}$$

For the linear case, we introduce the following equivalent notation:

$$\partial_t u + \mathcal{L}u = q, \quad x \in \Omega,\ t \in (0, T], \tag{5}$$

where $\mathcal{L}u$ is the linear advection-diffusion operator in conservation form:

$$\mathcal{L}u := \nabla \cdot (\boldsymbol{a}u - \mathbf{D}\nabla u), \tag{6}$$

and the advective velocity $\boldsymbol{a}$ and the diffusion tensor $\mathbf{D}$ are independent of u. The boundary and initial conditions are given by Equations (3)–(4), as before.

2.2 Weak form

The weak form of the mathematical problem relaxes the regularity requirements of the solution u. It is obtained by multiplying the differential equation by a smooth function v which vanishes on the boundary $\partial\Omega$, integrating over the entire domain Ω, and applying Green's formula to the flux term, to get the integral equation:

$$\int_\Omega \partial_t u\, v \,\mathrm{d}\Omega - \int_\Omega \boldsymbol{\mathcal{F}} \cdot \nabla v \,\mathrm{d}\Omega = \int_\Omega q v \,\mathrm{d}\Omega. \tag{7}$$

The relation above needs to be satisfied at each fixed time t for all functions v belonging to some appropriate space of functions $\mathcal{V}$. The choice of the functional space $\mathcal{V}$ depends on the form of the diffusion tensor and, for the purpose of this paper, it is sufficient to understand it as comprising smooth-enough functions which vanish on the boundary. The weak form of problem (1)–(4) is then stated succinctly as follows: seek $u \in \mathcal{V}$ for each fixed $t \in (0, T]$, such that

$$(\partial_t u, v) + a(u, v; u) = l(v) \quad \forall v \in \mathcal{V}, \tag{8}$$

where

$$(\partial_t u, v) := \int_\Omega \partial_t u \, v \, \mathrm{d}\Omega, \tag{9}$$

$$a(u, v; w) := -\int_\Omega \boldsymbol{\mathcal{F}} \cdot \nabla v \, \mathrm{d}\Omega = -\int_\Omega \boldsymbol{f}(w) \cdot \nabla v \, \mathrm{d}\Omega + \int_\Omega \mathbf{D}(w) \nabla u \cdot \nabla v \, \mathrm{d}\Omega, \tag{10}$$

$$l(v) := \int_\Omega q v \, \mathrm{d}\Omega. \tag{11}$$

The weak form of the *linear* problem given by (5)–(6) with boundary and initial conditions (3)–(4) is to find $u \in \mathcal{V}$ for each fixed $t \in (0, T]$, such that

$$(\partial_t u, v) + a(u, v) = l(v) \quad \forall v \in \mathcal{V}. \tag{12}$$

The only difference with respect to Equation (8) is that $a(u, v) \equiv a(u, v; u)$ is now a *bilinear* form.

2.3 Classical Galerkin method

With the notation above, it is straightforward to introduce the standard Galerkin approximation. The method consists in seeking a solution u_h in a finite-dimensional subspace $\mathcal{V}_h$ of the original (infinite-dimensional) space $\mathcal{V}$ such that, for each t:

$$(\partial_t u_h, v_h) + a(u_h, v_h; u_h) = l(v_h) \quad \forall v_h \in \mathcal{V}_h, \tag{13}$$

which constitutes a system of nonlinear ordinary differential equations. The fully discrete system is obtained by further discretizing in time.

The important point is that the *trial* functions u_h and the *test* functions v_h (usually piecewise polynomials) can only capture variability at a scale larger than the mesh resolution. All subgrid variability, *i.e.*, all features at a scale smaller than the element size, is automatically neglected. The well-known fact that the standard Galerkin method lacks stability for advection-dominated problems can be understood in this context. If the subscales are not captured adequately (or if they are completely ignored, as in the classical Galerkin method), their effects can propagate to larger scales, and deteriorate the coarse-scale calculations. In Section 3 we show examples of this behavior.

2.4 Multiscale approach

The fundamental principle of the multiscale approach is to acknowledge the presence of fine scales, which cannot be captured by the mesh. This is particularly important for advection-dominated problems, where the solution develops sharp features that would require an impractical grid resolution. The formulation is based on a multiple-scale decomposition of any function $v \in \mathcal{V}$ as [14]:

$$v = v_h + \tilde{v}, \tag{14}$$

where v_h is the part that can be resolved by the grid, and $\tilde{v}$ the unresolved part. This decomposition is unique if we can express the original functional space $\mathcal{V}$ as the direct sum of two spaces:

$$\mathcal{V} = \mathcal{V}_h \oplus \tilde{\mathcal{V}}, \tag{15}$$

where $\mathcal{V}_h$ is the space of *resolved scales* and $\tilde{\mathcal{V}}$ is the space of *subgrid scales*. The space $\tilde{\mathcal{V}}$ is an infinite-dimensional space that completes $\mathcal{V}_h$ in $\mathcal{V}$. This space is generally unknown, and it is the role of the subgrid model to provide a successful approximation to it.

For the **linear advection-diffusion problem**, the multiscale decomposition allows one to split the original problem into two. To this end, we express $u \equiv u_h + \tilde{u}$ in (12), and exploit the linearity of all the terms with respect to v. We obtain one equation for the *grid scales*,

$$(\partial_t(u_h + \tilde{u}), v_h) + a(u_h + \tilde{u}, v_h) = l(v_h) \quad \forall v_h \in \mathcal{V}_h, \tag{16}$$

and one for the *subscales*,

$$(\partial_t(u_h + \tilde{u}), \tilde{v}) + a(u_h + \tilde{u}, \tilde{v}) = l(\tilde{v}) \quad \forall \tilde{v} \in \tilde{\mathcal{V}}. \tag{17}$$

The former is a finite-dimensional problem, whereas the latter is infinite-dimensional.

In this investigation, the subscale problem is modeled using an algebraic subgrid-scale (ASGS) approximation (see [11, 17] for the details):

$$\tilde{u} \approx \tau \mathcal{R} u_h, \tag{18}$$

where $\mathcal{R}u_h := q - \partial_t u_h - \mathcal{L}u_h$ is the *grid-scale residual*, and the algebraic operator τ is called *intrinsic time* (or relaxation time). The expression of τ is one of the most difficult issues when devising stabilized methods. It should depend on the parameters of the problem, and on the actual discretization. From a numerical standpoint, a proper formulation of the intrinsic time should enhanced stability of the coarse-scale calculations without degrading the order of accuracy of the method. Here we use the following expression, which has proven useful in the context of linear systems of advection-diffusion-reaction equations [11]:

$$\tau = \left(c_1 \frac{\|\mathbf{D}\|}{h^2} + c_2 \frac{|\boldsymbol{a}|}{h} \right)^{-1}, \tag{19}$$

where h is a characteristic length of the element under consideration, and $c_1 = 4,\ c_2 = 2$ for linear elements [10, 11]. This completes the description of the subgrid scales.

After integration by parts on each element of the term $a(\tilde{u}, v_h)$ in Equation (16) and using a localization assumption [11], the equation for the grid scales takes the form:

$$(\partial_t u_h, v_h) + a(u_h, v_h) + \sum_e \int_{\Omega^e} \tilde{u}\, \mathcal{L}^* v_h \, \mathrm{d}\Omega = l(v_h) \quad \forall v_h \in \mathcal{V}_h, \tag{20}$$

where $\mathcal{L}^*$ is the adjoint of $\mathcal{L}$, defined in Equation (6). When compared with the standard Galerkin method, the multiscale approach involves additional integrals evaluated element by element (compare Equation (20) with Equation (13)), which incorporate the effect of the subgrid scales $\tilde{u}$ on the coarse scales. The subscales $\tilde{u}$ are modeled analytically and eliminated from the global problem. With the algebraic approximation used here, they are proportional to the grid scale residual (Equation (18)). The method is residual-based and, therefore, automatically consistent.

The new term in the grid-scale equation (20) is very similar to that of other stabilized formulations, the only difference being the form of the oper-

ator multiplying the subscales [10]:

$$\text{ASGS [14]:} \int_{\Omega^e} \tilde{u}\, \mathcal{L}^* v_h \, \mathrm{d}\Omega, \quad \mathcal{L}^* v := -\boldsymbol{a} \cdot \nabla v - \nabla \cdot (\mathbf{D} \nabla v), \tag{21}$$

$$\text{SUPG [5]:} \int_{\Omega^e} \tilde{u}\, (-\mathcal{L}_{\mathrm{adv}} v_h) \, \mathrm{d}\Omega, \quad -\mathcal{L}_{\mathrm{adv}} v := -\boldsymbol{a} \cdot \nabla v, \tag{22}$$

$$\text{GLS [16]:} \int_{\Omega^e} \tilde{u}\, (-\mathcal{L} v_h) \, \mathrm{d}\Omega, \quad -\mathcal{L} v := -\nabla \cdot (\boldsymbol{a} v) + \nabla \cdot (\mathbf{D} \nabla v). \tag{23}$$

The multiscale approach has several advantages over other stabilized formulations: (1) the stabilizing term arises naturally; (2) it is not restricted to a particular subgrid model; and (3) the ASGS formulation is endowed with better stability properties than SUPG and GLS [10, 11].

Extension of the multiscale approach to the **nonlinear problem** given by Equations (1)–(4) is not straightforward, mainly because the form $a(u, v; w)$ in Equation (8) is not linear in w. We propose an incremental formulation and a multiple scale decomposition of the increment [17]:

$$u \approx u_h + \delta\tilde{u}. \tag{24}$$

The incremental subscale $\delta\tilde{u}$ may be understood as a perturbation. Since the form $a(u, v; w)$ is linear with respect to the second argument (test function), the multiscale approach leads also to a grid-scale problem and a subscale problem. Expanding the constitutive relations $\boldsymbol{f}(u)$ and $\mathbf{D}(u)$ to first order about an approximate coarse-scale solution u_h, we obtain equations which are formally identical to those of the linear case (see [17] for the derivation), except that now involve a *linearized* advection-diffusion operator:

$$\mathcal{L}_{u_h} v := \nabla \cdot \left[\boldsymbol{f}'(u_h) - \mathbf{D}'(u_h) \nabla u_h - \mathbf{D}(u_h) \nabla v \right]. \tag{25}$$

In particular, the equation for the incremental subscales reads:

$$\delta\tilde{u} \approx \tau_{u_h} \mathcal{R}(u_h), \tag{26}$$

where τ_{u_h} (intrinsic time) is now a nonlinear function of the grid scale solution u_h. The coarse-scale equation reads

$$(\partial_t u_h, v_h) + a(u_h, v_h; u_h) + \sum_e \int_{\Omega^e} \delta\tilde{u}\, \mathcal{L}^*_{u_h} v_h \, d\Omega = l(v_h) \quad \forall v_h \in \mathcal{V}_h, \tag{27}$$

where $\mathcal{L}^*_{u_h}$ is the adjoint of the *linearized* operator $\mathcal{L}_{u_h}$, defined in Equation (25). Equations (26) and (27) describe the algebraic subgrid scale finite element method for a nonlinear advection-diffusion equation, and are analogous to Equations (18) and (20) for the linear case. In the nonlinear case, however, these equations need to be solved using an iterative procedure, such as Newton's method.

3 Representative numerical simulations

In this section we present some numerical simulations of miscible and immiscible flow. For simplicity, we shall concentrate on the one-dimensional problem. Therefore, the flux vector and the diffusion tensor reduce to scalar quantities. It is not the purpose of this paper to derive the equations for miscible and immiscible flow (see [17] and the references therein for a derivation).

3.1 One-dimensional miscible flow

We consider one-dimensional flow of a tracer that is perfectly miscible with water. Under certain assumptions, the governing equation of tracer transport is a transient linear advection-diffusion-reaction equation:

$$\partial_t u + v_T \partial_x u - D\partial_{xx} u + \sigma u = q, \quad x \in (0, L),\ t \in (0, T] \tag{28}$$

where u is the mass fraction of the tracer (tracer concentration), v_T is the total velocity of the mixture, D is the diffusion coefficient, σ is the decay constant for a radioactive tracer, q is the distributed source term, and L is the length of the 1D domain. The diffusion coefficient D is taken as a constant, thus neglecting the effects of hydrodynamic dispersion. We intentionally do not account for dispersion because it would smear out the fronts, thus reducing considerably the numerical complexity of the problem.

We solve the problem with homogeneous Dirichlet boundary conditions:

$$u(0, t) = u(L, t) = 0, \tag{29}$$

Diffusion	Advection	Reaction
$\tau_d = \dfrac{h^2}{4D}$	$\tau_a = \dfrac{h}{2v_T}$	$\tau_r = \dfrac{1}{\sigma}$

Table 1. Expressions of the characteristic times for advection, diffusion and reaction processes, taking as a reference length one-half of the element size.

and the following parameters: $L = 10$, $D = 10^{-3}$, $q = 1$. We investigate two test cases, each one with different advective velocities v_T and reaction coefficients σ:

1. Dominant advection: $v_T = 1,\ \sigma = 0$.
2. Advection and reaction: $v_T = 1,\ \sigma = 4$.

In both cases we used a very coarse uniform grid of 40 linear elements (the element size is $h = 0.25$), and a backward Euler time-stepping scheme with constant time step $\delta t = 0.1$.

It is illustrative to compute the intrinsic times for each of the physical processes involved, taking as a reference length one-half of the element size. The expressions for the characteristic times are given in **Table 1**. From the intrinsic times, the Courant, Peclet and Damkholer numbers can be calculated for each of the test cases (see **Table 2**). The *Courant number* indicates whether the time discretization is fine enough to simulate the quickest process. It is usually restricted to be less than 1.0 for stability or accuracy requirements. The *Peclet* and *Damkholer numbers* measure, respectively, the preeminence of advection and reaction with respect to diffusion. Values of these dimensionless numbers much greater than 1.0 imply that the problem is *not* dominated by diffusion, suggesting that the solution might present sharp features.

The expression of the intrinsic time used in the subgrid model (18) is the harmonic mean of the characteristic time of each process [11], *i.e.*,

$$\tau = \left(\tau_d^{-1} + \tau_a^{-1} + \tau_r^{-1}\right)^{-1} = \left(4\frac{D}{h^2} + 2\frac{v_T}{h} + \sigma\right)^{-1}. \tag{30}$$

	Courant # $Co := \delta t/\tau_{\min}$	Peclet # $Pe := \tau_d/\tau_a$	Damkholer # $Da := \tau_d/\tau_r$
1. Dominant advection	0.8	125	0
2. Advection-reaction	0.8	125	67.5

Table 2. Courant, Peclet, and Damkholer dimensionless numbers for each test case of the linear advection-diffusion-reaction problem.

The expression above generalizes Equation (19) for cases when a reaction term is present, and provides a physical interpretation of the intrinsic time used in the multiscale approach.

3.1.1 Test Case 1: Dominant advection

The governing equation is ($\sigma = 0$ in Equation (28)):

$$\partial_t u + v_T \partial_x u - D\partial_{xx} u = q, \tag{31}$$

and the concentration is initially zero everywhere. For **early times**, the behavior of the solution is as follows:

1. *Away from both boundaries.* Because the initial concentration is uniform, and so is the source term, the concentration gradients will be zero as long as the region is not affected by the boundaries. Since $\partial_x u \approx 0$, the equation reduces to:

   $$\partial_t u \approx q. \tag{32}$$

   Therefore, the solution consists in a *plateau*, rising at a rate of $q = 1$ concentration units per unit time.

2. *Near the left (inlet) boundary.* Physically, what happens is that water with zero concentration from the inlet boundary "washes" water with tracer inside the domain. A steady tracer profile is established near the inlet, accommodating the effects of advection and distributed source. Since the concentration profile is steady ($\partial_t u \approx 0$) and diffusion is negligible ($D \approx 0$), the approximate governing equation for this conditions

is:

$$v_T \partial_x u \approx q. \tag{33}$$

The solution near the left boundary is, thus, a *ramp* of slope $q/v_T = 1$.

3. *Near the right (outlet) boundary.* In the neighborhood of this boundary, diffusion cannot be ignored. A *boundary layer* develops to connect the solution far away from the boundary (given by the rising plateau) to the Dirichlet boundary condition. The width of this layer is of the order of $D/v_T = 10^{-3}$.

For **long simulation times**, steady-state conditions are reached when the effect of the inlet boundary is felt at the outlet. The solution then consists of a ramp of slope $q/v_T = 1$ and a sharp boundary layer of width $\sim D/v_T = 10^{-3}$.

Solution by the Galerkin method and the algebraic subgrid scale (ASGS) method are shown in **Figure 1** at three different times ($t = 2$, $t = 5$, and steady-state). At time $t = 2$, the standard Galerkin solution is wildly oscillatory. Oscillations are more pronounced near the outlet face, but significant in more than half of the computational domain. For later times, the solution is globally polluted with nonphysical oscillations. The oscillatory behavior arises because the method lacks stability: the boundary layer cannot be resolved with the discretization used (the boundary layer width is two orders of magnitude smaller than the element size), and this loss of accuracy at the subgrid scale "propagates" to degrade the coarse-scale calculations.

On the other hand, the solution obtained by the ASGS method is perfectly nonoscillatory. The calculated concentration profiles reproduce the transient behavior described above: a ramp near the inlet boundary, a rising plateau in the center region, and a sharp layer at the outlet boundary. The slope of the ramp and the rate of increase of the plateau concentration agree with the predicted values. Moreover, the boundary layer is reproduced in the best possible way given the actual discretization: it is captured with just one element, and without a single overshoot.

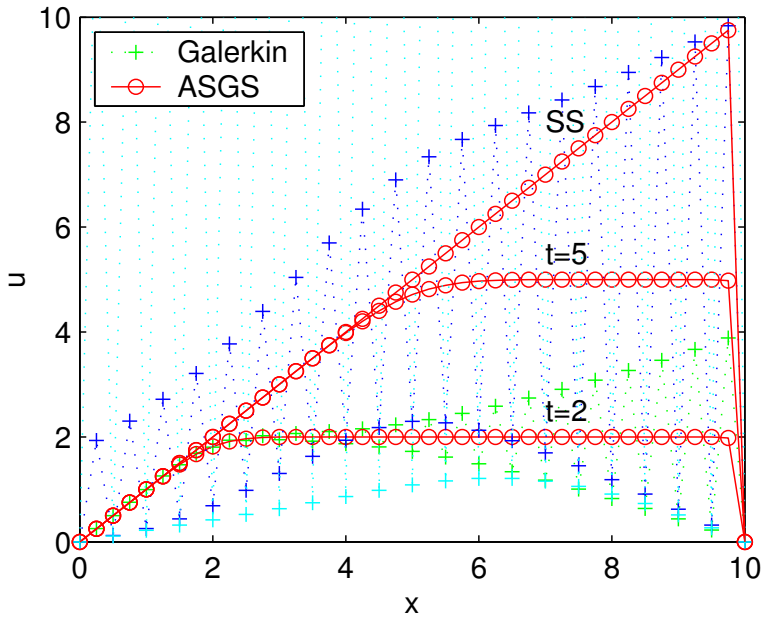

Figure 1. Linear advection-diffusion-reaction with sources. Test case 1: dominant advection. ASGS vs. Galerkin solutions at three different times.

3.1.2 Test Case 2: Dominant advection and reaction

The governing equation is the full Equation (28), with zero initial and boundary conditions. We can identify the following features in the solution:

1. *Away from both boundaries.* Using the same arguments as before, this is a region of uniform concentration u_*, described by the initial value problem:
$$\frac{\mathrm{d}u_*}{\mathrm{d}t} + \sigma u_* = q, \quad u_*(t=0) = 0. \tag{34}$$
The solution is:
$$u_* = \frac{q}{\sigma}\left(1 - e^{-\sigma t}\right), \tag{35}$$
so the rising plateau tends asymptotically to a steady value of $q/\sigma = 0.25$.

2. *Near the left (inlet) boundary.* It is difficult to obtain an analytical description of the solution during the transient phase. However, when steady-state conditions are reached ($\partial_t u = 0$) and neglecting the effects of diffusion, the governing equation reduces to:
$$v_T \frac{\mathrm{d}u}{\mathrm{d}x} + \sigma u = q, \quad u(x=0) = 0. \tag{36}$$
The solution to the problem above is the concentration profile:
$$u = \frac{q}{\sigma}\left(1 - e^{-\frac{\sigma}{v_T}x}\right), \tag{37}$$
The width of this profile can be estimated by the value of x such that $u \approx 0.95 u_{\max}$, which gives a width of ~ 0.75.

3. *Near the right (outlet) boundary.* The solution consists of a boundary layer with the same characteristics as that of Case 1.

In **Figure 2** we show the results obtained with the classical Galerkin method and the ASGS approach, at three different times ($t = 0.2$, $t = 0.4$, and steady-state). The standard Galerkin solution reproduces the rising plateau, and it captures the structure of the solution at the left boundary. We recall that, for the parameters used in this simulation, the concentration

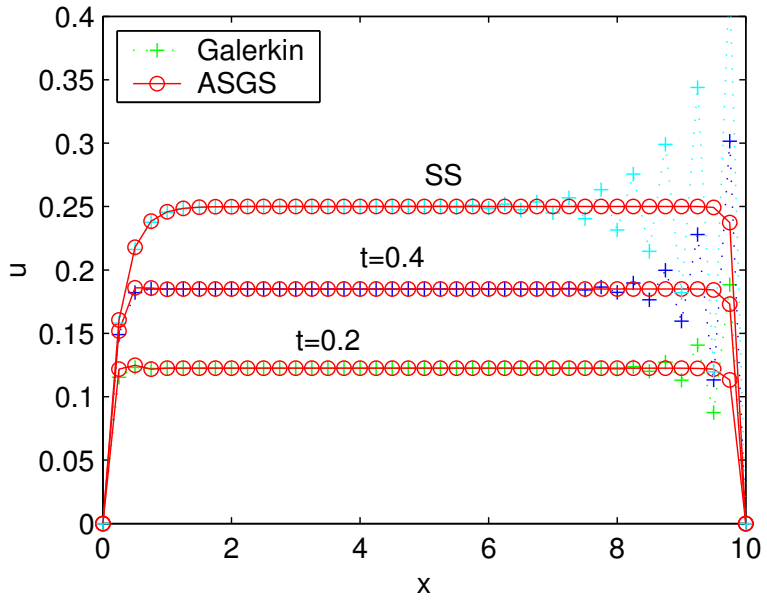

Figure 2. Linear advection-diffusion-reaction with sources. Test case 2: combination of advection and reaction. ASGS vs. Galerkin solutions at three different times.

profile at the inlet has a width of the order of 2 or 3 elements. However, the classical Galerkin method displays nonphysical oscillations at the right end, which propagate well into the domain. This nonlocal oscillatory behavior denotes the lack of stability of the method, and its inability to appropriately "damp out" subgrid effects.

By contrast, the ASGS solution is accurate and stable: it captures sharply all the features of the solution, and does not present spurious oscillations. It is important to note that the ASGS formulation does not introduce additional computational cost with respect to the classical Galerkin method.

3.2 One-dimensional immiscible flow

Flow of two incompressible immiscible fluids ignoring gravitational effects is described, using the fractional-flow approach [8], by an elliptic "pressure" equation and a parabolic "saturation" equation. In the one-dimensional case, the pressure equation has a trivial solution, as the total velocity depends

only on the boundary conditions (see [8, 17] for the details). The saturation equation takes the form of a nonlinear advection-diffusion scalar conservation law:

$$\partial_t u + \partial_x \left(f(u) - D(u)\partial_x u \right) = q, \quad x \in (0, L),\ t \in (0, T], \tag{38}$$

where u is the water saturation, q is the distributed source term. Functions f and D take the following expressions:

$$f(u) = v_T \frac{\lambda_w}{\lambda_w + \lambda_o}, \tag{39}$$

$$D(u) = \frac{\lambda_w \lambda_o}{\lambda_w + \lambda_o} \frac{k}{\phi} \left(-P_c' \right), \tag{40}$$

where v_T is the total velocity (assumed constant and known from the pressure equation), λ_α is the mobility of the α-phase, k is the intrinsic permeability, ϕ is the porosity, and P_c' is the derivative of the capillary pressure with respect to saturation. The fractional flow function f is typically S-shaped and, thus, nonconvex. We shall consider the following model [12, 18] (**Figure 3**):

$$f(u) = v_T \frac{u^2}{u^2 + \mu(1-u)^2}, \tag{41}$$

where μ is the viscosity ratio, taken here as 1. The diffusion coefficient D, which arises from capillarity effects, is typically degenerate at the endpoint saturations, *i.e.*, it vanishes for $u = 0$ and $u = 1$, and is positive otherwise [8]. To mimic this behavior, we choose the following expression [12] (**Figure 4**):

$$D(u) = \epsilon u(1-u). \tag{42}$$

We solve Equation (38) on the unit segment $\Omega = [0, 1]$ with Dirichlet boundary conditions $u(0, t) = 1,\ u(1, t) = 0$, and zero initial conditions. The total flux is $v_T = 1$, the distributed source term is $q = 0$, and the constant in the degenerate diffusion coefficient is $\epsilon = 10^{-4}$. We used a very small value of ϵ to minimize the effects of capillary pressure and solve the near-hyperbolic problem.

The diffusion-free problem, or Buckley-Leverett problem [6], admits a straightforward analytical solution. During the **transient phase** (before breakthrough), the solution consists of a rarefaction fan and a shock. Both

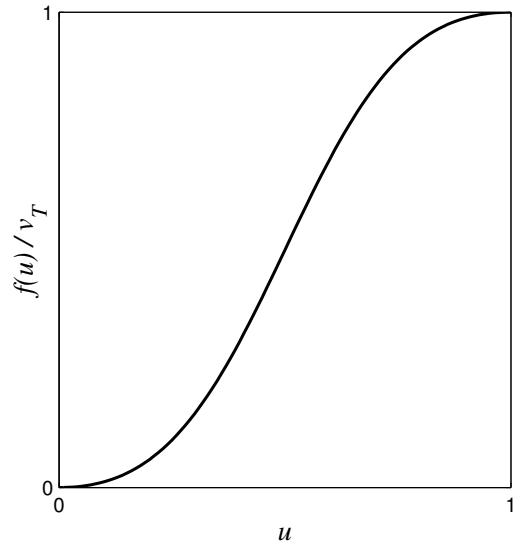

Figure 3. Fractional flow function f used in the immiscible flow simulations. The function is typically S-shaped and, thus, nonconvex.

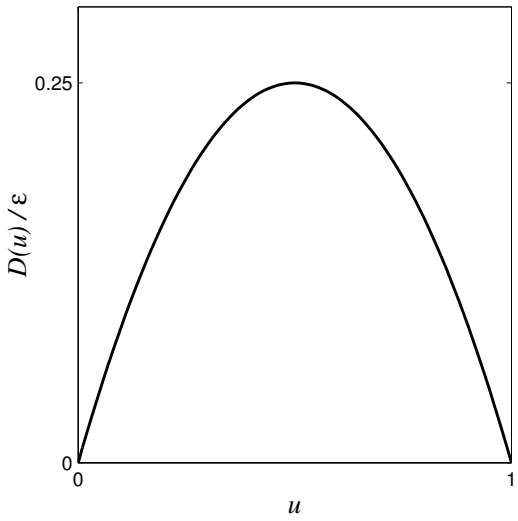

Figure 4. Capillary diffusion function D used in the immiscible flow simulations. The function typically vanishes at the endpoint saturations, and is positive elsewhere.

the shock speed and the post-shock value are constant, and easily computable from the flux function [18]. As a result, the solution "stretches" with time in a self-similar fashion. For **long simulation times** (after breakthrough), the system reaches a quasi-steady state. Dirichlet boundary conditions are particularly challenging, because they force a very fast initial transient at the inlet, and a sharp boundary layer at the outlet after breakthrough. This problem "exhibits several difficult features beyond the usual ones of advection-dominated flow: degenerate diffusion, sharpening near-shock solutions, and capillary outflow boundary layers" [12]. Numerical solutions to the Buckley-Leverett problem include the early works of Todd *et al.* [20], Aziz and Settari [2,19] and, more recently, Dahle *et al.* [12], and Binning and Celia [3].

Since we use a very small value of the parameter ϵ, capillary diffusion effects do not greatly influence the *global* structure of the solution. However, capillarity is *not* negligible in the neighborhood of sharp features, because of the extremely high saturation gradients. In particular, the width of the traveling shock (before breakthrough) and the boundary layer at the outlet face (after breakthrough) are of the order of $\epsilon/v_t = 10^{-4}$. Of course, resolving the fine-scale structure of the solution would require elements smaller than this length. This is not feasible in practical problems, and the goal is to obtain an accurate numerical solution on a coarse grid, which preserves the global structure of the exact solution.

Results for a very coarse grid ($N_e = 20,\ \delta t = 0.01$, **Figure 5**) and a finer grid ($N_e = 500,\ \delta t = 0.0005$, **Figure 6**) are provided, which correspond to element Peclet numbers of $Pe \approx 2,500$ and $Pe \approx 100$, respectively.[1] In all cases we used a backward Euler time-stepping scheme. The expression of the relaxation time used in the ASGS formulation is:

$$\tau_{u_h} = \left(\tau_d^{-1} + \tau_a^{-1}\right)^{-1} = \left(4\frac{D(u_h)}{h^2} + 2\frac{a(u_h)}{h}\right)^{-1}, \tag{43}$$

where the "advective velocity" $a(u_h)$ comes from the proposed linearization

[1] This range of Peclet numbers is to be compared with that of simulations using characteristics methods [3,12], where the highest Peclet number considered is about 2.

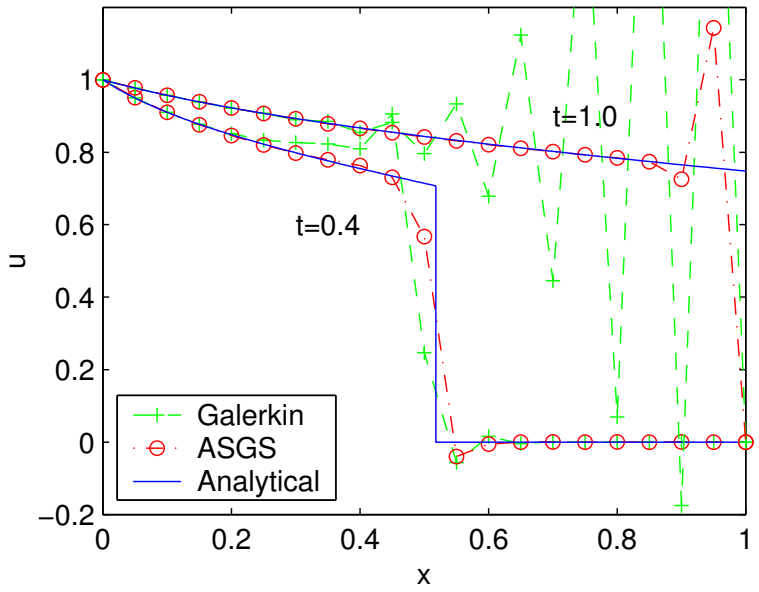

Figure 5. One-dimensional immiscible flow. The classical Galerkin solution and the ASGS solution on a *very coarse grid* (20 linear elements) are compared with the Buckley-Leverett solution for transient and quasi-steady conditions.

of the problem, and is given by:

$$a(u_h) = f'(u_h) + D'(u_h)\partial_x u_h. \tag{44}$$

In **Figure 5**, the numerical solutions obtained by the standard Galerkin method and the ASGS method on the coarse grid are compared with the analytical solution of the hyperbolic problem. The classical Galerkin method produces a big overshoot and a nonphysical saturation plateau upstream of the front during the transient state (shown is a snapshot of the solution at $t = 0.4$). More noticeably, it gives a completely oscillatory solution after breakthrough (the results are displayed at $t = 1$). On the other hand, the ASGS solution is *not* globally polluted with oscillations, and preserves a sharp definition of the saturation front and the boundary layer. The ASGS solution is remarkably accurate wherever the actual solution is smooth (*i.e.*, along the rarefaction fan), even though an extremely coarse mesh of just 20 linear elements was used. The oscillatory behavior of the

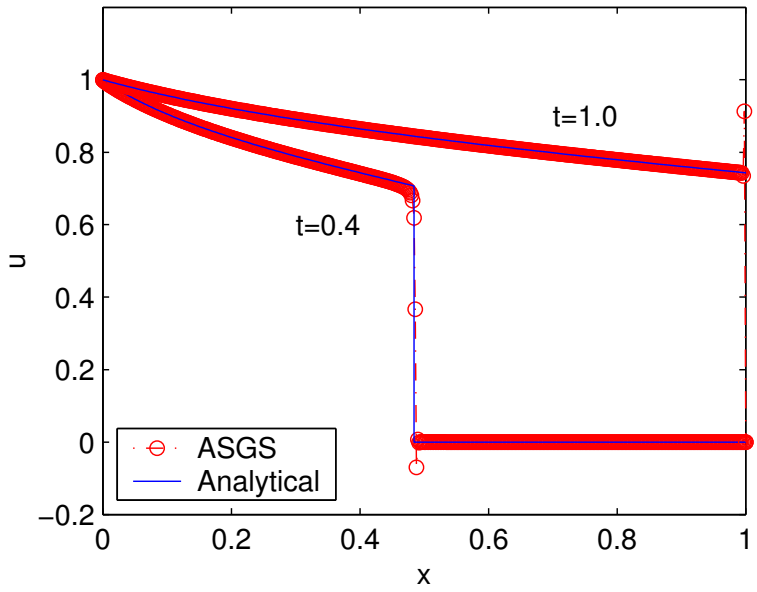

Figure 6. One-dimensional immiscible flow. The ASGS solution on a *finer grid* (500 linear elements) is compared with the Buckley-Leverett solution for transient and quasi-steady conditions. The classical Galerkin method did not converge for $t = 1$.

numerical solution is confined to a single undershoot at the downstream end of the traveling shock, and a single overshoot at the boundary layer for the long-time solution.

These observations are further confirmed by the simulations on a finer grid (500 linear elements, **Figure 6**). In this case, the standard Galerkin method did not converge at all for $t = 1$ and, thus, is not shown in the figure. The most important feature of the ASGS solution is that the advancing front (before breakthrough) and the boundary layer (after breakthrough) are captured sharply, avoiding the excessive smearing of traditional upwind formulations. The localized wiggles that remain in the solution can be successfully removed by using a shock-capturing technique [17], which introduces numerical dissipation only in the neighborhood of discontinuities [9].

A Newton scheme was used in all cases to solve the system of nonlinear algebraic equations. In **Figure 7** we show the evolution of the L_2-norm of

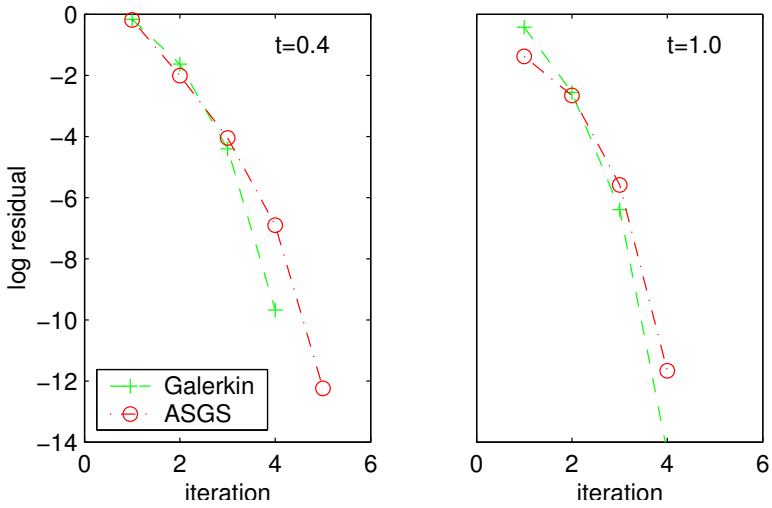

Figure 7. One-dimensional immiscible flow. Evolution of the Newton iterative scheme for the standard Galerkin and ASGS methods on the coarse grid, for two typical time steps ($t = 0.4$ and $t = 1$). Convergence is monotinic and quadratic in both cases.

the residual for two typical time steps ($t = 0.4$ for transient conditions, and $t = 1.0$ for quasi-steady conditions) of the coarse grid simulations. The main observation is that convergence is monotonic and asymptotically quadratic for both methods (classical Galerkin and ASGS). The additional stabilizing term of the ASGS formulation does not degrade convergence of the Newton iterative scheme. On the contrary, convergence of the ASGS method on the finer grid is also quadratic at all times, whereas the standard Galerkin method fails to converge shortly after breakthrough, due to unbounded growth of spurious oscillations.

4 Conclusions

We have presented a paradigm for the numerical solution of nonlinear conservation laws, which is based on a multiscale decomposition of the variable of interest, and applied it to the problems of miscible and immiscible two-phase flow in porous media. The main idea is to acknowledge that the fine-scale

structure of the solution cannot be captured by any grid, and to incorporate the net effect of the subgrid scales onto the scales resolved by the mesh [14,15]. An algebraic approximation of the subscales [11] is used to model subgrid variability. The key parameter of the formulation is the intrinsic time τ, which is calculated as the harmonic mean of the characteristic times of diffusion, advection and reaction at the length scale of the element size. This multiscale approach leads to stabilized finite element methods with excellent properties. To the best of our knowledge, this approach is entirely new in the context of flow in porous media.

The formalism of the multiscale approach is very general, and several issues need to be investigated further. Of particular interest is the development of alternative subscale models. In this paper, we focussed our attention on the efficient numerical solution of *standard* mathematical formulations of miscible and immiscible flow. The only link to the physical processes at the micro-scale was through the expression we used for the intrinsic time. The multiscale framework could be used, however, to incorporate *physically-based* models of micro-scale processes in the field-scale equations.

From the standpoint of numerical methods, the multiscale approach constitutes also a paradigm for *a posteriori* error estimation [1], shock-capturing techniques [17], and temporal integration [4]. We are now extending this methodology to multiphase compositional flows in several dimensions.

Nomenclature

Roman letters

$a(\cdot,\cdot,\cdot) =$ form in the weak formulation

$\boldsymbol{a} =$ advective velocity, L/t

$c_1, c_2 =$ constants in the definition of τ, dimensionless

$Co =$ Courant number, dimensionless

$\mathbf{D} =$ diffusion tensor, L^2/t

$Da =$ element Damkholer number, dimensionless

$\boldsymbol{f} =$ hyperbolic part of the flux $\boldsymbol{\mathcal{F}}$, L/t

$\boldsymbol{\mathcal{F}} =$ total flux of u, L/t

$h =$ characteristic length of an element, L

$\mathbf{k} =$ absolute permeability tensor, L^2

$\mathcal{L} =$ linear advection-diffusion operator, 1/t

$\mathcal{L}^* =$ adjoint of $\mathcal{L}$, 1/t

$\mathcal{L}_{u_h} =$ linearized advection-diffusion operator, 1/t

$\mathcal{L}^*_{u_h} =$ adjoint of $\mathcal{L}_{u_h}$, 1/t

$l(\cdot) =$ linear form in the weak formulation

$N_e =$ number of elements, dimensionless

$P_c =$ capillary pressure, $\mathrm{m/Lt}^2$

$Pe =$ element Peclet number, dimensionless

$q =$ distributed source term of u, 1/t

$\mathcal{R}(u_h) =$ grid-scale residual, 1/t

$t =$ time, t

$T =$ time interval, t

$u =$ generic conserved quantity, dimensionless

$u_h =$ grid-scale part of u, dimensionless

$\tilde{u} =$ subgrid-scale part of u, dimensionless

$u_0 =$ initial conditions of u, dimensionless

$\boldsymbol{v}_T =$ total fluid velocity, L/t

$\mathcal{V} =$ space of trial and test functions

$\mathcal{V}_h =$ space of grid-scale functions

$\tilde{\mathcal{V}} =$ space of subgrid scales

$x =$ space coordinate, L

Greek letters

$\delta =$ increment

$\lambda_w,\ \lambda_o =$ relative mobility of water and oil, Lt/m

$\mu =$ viscosity ratio, dimensionless

$\tau =$ relaxation time, t

$\phi =$ porosity, dimensionless

$\Omega =$ spatial domain, L in 1D, L^2 in 2D, L^3 in 3D

$\partial\Omega =$ boundary of the domain

ACKNOWLEDGEMENTS

This work was supported in part by the U.S. Department of Energy under Contract No. DE-AC03-76SF00098. Funding provided by the Jane Lewis fellowship and the Repsol-YPF fellowship, awarded to the first author, are gratefully acknowledged.

References

[1] M. Ainsworth and J. T. Oden. *A Posteriori Error Estimation in Finite Element Analysis*. John Wile & Sons, New York, 2000.

[2] K. Aziz and A. Settari. *Petroleum Reservoir Simulation*. Elsevier, London, 1979.

[3] P. Binning and M. A. Celia. Practical implementation of the fractional flow approach to multi-phase flow simulation. *Adv. Water Resour.*, 22(5):461–478, 1999.

[4] C. L. Botasso. Multiscale temporal integration. *Comput. Methods Appl. Mech. Engrg.*, 191:2815–2830, 2002.

[5] A. N. Brooks and T. J. R. Hughes. Streamline upwind Petrov-Galerkin formulations for convection dominated flows with particular emphasis on the incompressible Navier-Stokes equations. *Comput. Methods Appl. Mech. Engrg.*, 32:199–259, 1982.

[6] S. E. Buckley and M. C. Leverett. Mechanism of fluid displacement in sands. *Petrol. Trans.* AIME, 146:107–116, 1942.

[7] M. A. Celia, T. F. Russell, I. Herrera, and R. E. Ewing. An Eulerian-Lagrangian localized adjoint method for the advection-diffusion equation. *Adv. Water Resour.*, 13(4):187–206, 1990.

[8] G. Chavent and J. Jaffré. *Mathematical Models and Finite Elements for Reservoir Simulation*, volume 17 of *Studies in Mathematics and its Applications*. Elsevier, North-Holland, 1986.

[9] R. Codina. A discontinuity-capturing crosswind-dissipation for the finite element solution of the convection-diffusion equation. *Comput. Methods Appl. Mech. Engrg.*, 110:325–342, 1993.

[10] R. Codina. Comparison of some finite element methods for solving the diffusion-convection-reaction equation. *Comput. Methods Appl. Mech. Engrg.*, 156:185–210, 1998.

[11] R. Codina. On stabilized finite element methods for linear systems of convection-diffusion-reaction equations. *Comput. Methods Appl. Mech. Engrg.*, 188:61–82, 2000.

[12] H. K. Dahle, R. E. Ewing, and T. F. Russell. Eulerian-Lagrangian localized adjoint methods for a nonlinear advection-diffusion equation. *Comput. Methods Appl. Mech. Engrg.*, 122:223–250, 1995.

[13] R. E. Ewing. *Mathematics of Reservoir Simulation*, volume 1 of *Frontiers in Applied Mathematics*. SIAM, Philadelphia, 1983.

[14] T. J. R. Hughes. Multiscale phenomena: Green's functions, the Dirichlet-to-Neumann formulation, subgrid scale models, bubbles and the origins of stabilized methods. *Comput. Methods Appl. Mech. Engrg.*, 127:387–401, 1995.

[15] T. J. R. Hughes, G. R. Feijóo, L. Mazzei, and J.-B. Quincy. The variational multiscale method—a paradigm for computational mechanics. *Comput. Methods Appl. Mech. Engrg.*, 166:3–24, 1998.

[16] T. J. R. Hughes, L. P. Franca, and G. M. Hulbert. A new finite element formulation for computational fluid dynamics: VIII. The Galerkin least-squares method for advective-diffusive equations. *Comput. Methods Appl. Mech. Engrg.*, 73:173–189, 1989.

[17] R. Juanes and T. W. Patzek. Multiple scale stabilized finite elements for the simulation of tracer injections and waterflood. In *SPE/DOE Thirteenth Symposium on Improved Oil Recovery*, Tulsa, OK, April 13–17, 2002. (SPE 75231).

[18] R. J. LeVeque. *Numerical Methods for Conservation Laws*. Birkhäuser Verlag, Berlin, second edition, 1992.

[19] A. Settari and K. Aziz. Treatment of nonlinear terms in the numerical solution of partial differential equations for multiphase flow in porous media. *Int. J. Multiphase Flow*, 1:817–844, 1975.

[20] M. R. Todd, P. M. O'Dell, and G. J. Hirasaki. Methods of increased accuracy in numerical reservoir simulators. *SPEJ*, 12(6):515–530, December 1972. *Petrol. Trans.* AIME, 253.